Electrochemical Nitric Oxide Reduction on Metal Surfaces

Hao Wan, Alexander Bagger, and Jan Rossmeisl*

Center for High Entropy Alloy Catalysis (CHEAC), Department of Chemistry, University of Copenhagen, Universitetsparken 5, DK-2100 Copenhagen, Denmark

E-mail: Jan.Rossmeisl@chem.ku.dk

Abstract

Electrocatalytic denitrification is a promising technology for removing NO_x species (NO_3^-, NO_2^- and NO). For NO_x electroreduction (NO_xRR), there is a desire for understanding the catalytic parameters that control the product distribution. Here, we elucidate selectivity and activity of catalyst for NO_xRR. At low potential we classify metals by the binding of $*$NO versus $*$H. Analogous to classifying CO_2 reduction by $*$CO vs $*$H, Cu is able to bind $*$NO while not binding $*$H giving rise to a selective NH_3 formation. Besides being selective, Cu is active for the reaction found by an activity-volcano. For metals that does not bind NO the reaction stops at NO, similar to CO_2-to-CO. At potential above 0.3 V vs RHE, we speculate a low barrier for N coupling with NO causing N_2O formation. The work provide a clear strategy for selectivity and aims to inspire future research on NO_xRR.

Keywords

NO_x Removal, Ammonia Synthesis, Metal Surfaces, DFT, Electrocatalysis

Introduction

Nitrogen can be transformed through biological and physical processes within the nitrogen cycle to form a broad spectrum of inorganic compounds, including ammonia (NH_3), hydrazine (N_2H_4), hydroxylamine (NH_2OH), nitrite (NO_2^-), nitrate (NO_3^-), nitric oxide (NO), and nitrous oxide (N_2O).[1,2] While many of these processes are essential to life, large-scale commercial food production has led to over-fertilization and consequent accumulation of nitrate and nitrite ions in groundwater and in agricultural runoff streams. Both nitrate and nitrite ions are a source of pollution in groundwater, lakes, and coastal water, causing serious health problems, such as methemoglobinemia and cancer, when ingested in high concentrations.[3–5] As a result, groundwater treatments to reduce the concentration of these ions have been developed and have become an important environmental consideration.[6,7]

Meanwhile, the artificial N_2 fixation towards NH_3 is produced via the Haber-Bosch process. In the Haber-Bosch process, NH_3 is produced in a reaction between H_2 and N_2 at high pressure and temperature. As a consequence, the Haber-Bosch process depends on the use of gaseous H_2 which is commonly made from fossil fuel steam methane reforming (SMR). By contrast, the electrochemical conversion of NO_x (x = 1, 2, and 3) to NH_3 involves only H^+ and electrons from electricity that can be from sustainable sources, like wind and solar energy.

Electrochemical denitrification is a promising strategy for the removal of NO_x species from waste-water and constitutes a plausible alternative to traditional denitrification methods, such as biological and physical separations processes, due to its environmental compatibility, energy efficiency, safety, product selectivity, and potential for use in smaller-scale devices.[6–15] Nitrate and nitrite electroreduction can produce a variety of products, such as N_2, N_2O, NH_3, and NH_2OH.[7,9,16,17] The reduction of NO is an essential environmental reaction, since it determines the performance of waste-water treatment catalysts for NO_3^-, NO_2^- and NO removal.[6,7]

Investigating electrochemical NO reduction (NORR) is a first step toward understanding

the fundamentals of electrocatalytic NO_3^-/NO_2^- reduction and developing improved electrochemical denitrification or even sufficient NH_3 production technologies.[6,7,9,18–20] In addition, the study of NO electrochemistry is of fundamental scientific interest because observations and developed methods can be straightforwardly applied to other environmentally friendly electrocatalytic reduction chemistries. Indeed, as we will show, the electrochemistry of NO has numerous analogies to CO_2/CO electroreduction, which has been reported before.[21,22]

In this work, we study the potential dependence of the electrocatalytic reduction of NO among a group of metals via density functional theory (DFT) simulations. Electrochemical NO reduction is complicated reaction, and in this work, we aim to understand the reaction and capture the main features of the reaction, which can enable us to find promising catalysts without knowing all the reactions details, such as kinetics. The ideal scenario of all electrocatalysts is that a catalyst can conduct the reaction at low overpotential and with acceptable rates and faradaic efficiency. For NORR at catalyst potential, just above HER, NH_3 formation has been reported with fairly high Faradaic efficiency.[14,23,25,31] However, at these potentials a relatively low rate is obtained, simply due to the slow HER. In addition, Increasing the overpotential to speed up the reaction, is not possible since this leads to a significant increase in H_2 evolution and as a result the Faradaic efficiency quick drops.[14,26,31] In conclusion, the scenario that we try to cover in our selective scheme is the case where selective NH_3 formation from NORR is obtained with acceptable rate with a normal surface area catalyst. We note that rates will depend on the number of active sites; if a high surface area catalyst is used, sufficient rates could in principle be obtained prior to HER with acceptable Faradaic efficiency. Here, we classify metals for the electrochemical reduction of NO_3^-/NO_2^-/NO, to understand what surface properties determine the main product during reduction, which has been found to be: H_2, NH_3, N_2 and N_2O. The classification scheme for NO_3^-/NO_2^-/NO reduction is applied to understand products distribution without knowing the mechanism, while NO_3^-/NO_2^- reduction is beyond the scope. The analysis has been split into two potential regions according to experimental results as shown in Fig. 1: low

and high potential. In each potential region, a descriptor-based method has been utilized to explain experimental observations of the various products formation. Especially under low potential, activity volcano has been constructed against the adsorption energy of ∗N, and Cu has been demonstrated as the most selective and active metal here for NO reduction since it adsorbs ∗NO but not ∗H.

Our working hypothesis is that the binding energies of relevant intermediates will determine trends in catalytic properties of each metal catalyst. This is under the assumption that (a) the interaction between metals and the electrochemical environment is similar; (b) the trends in low-coverage regime capture the most important features of the catalyst performance; (c) the classification is assumed to be within the major products.

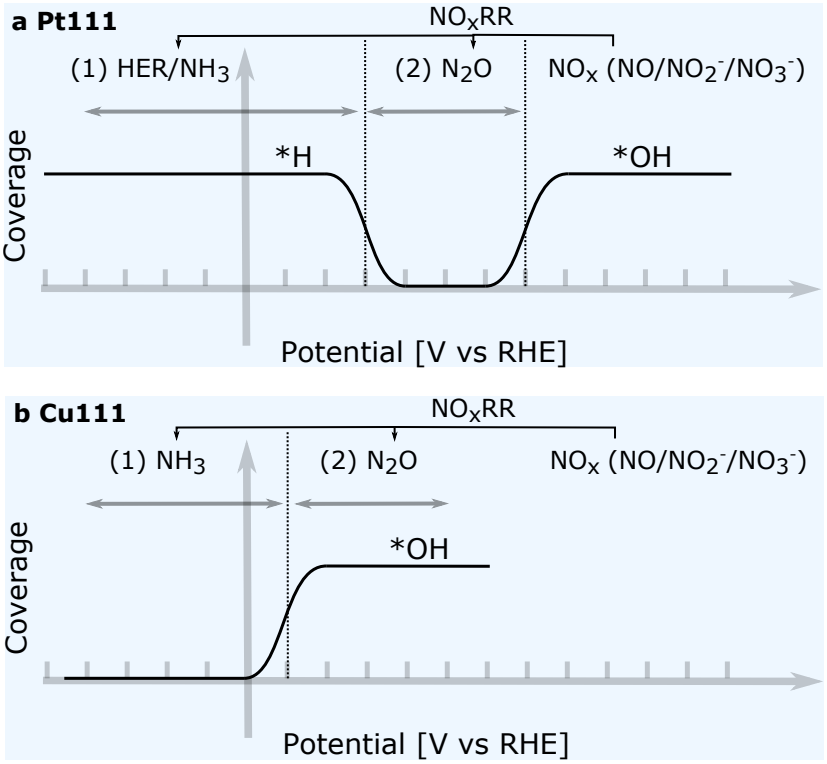

Figure 1: Schematic representation of experimental products from NO reduction on (a) Pt(111) and (b) Cu(111) and the relation to surface coverage. Two potential regions are shown with different product formation.

Electrochemical reduction of NO_3^-/NO_2^-/NO

The electrochemical conversion of NO_3^- under reduction condition is complex, involving multiple reactions, products and stable intermediates (e.g., ammonia, nitrite, hydroxylamine, nitric oxide, nitrous oxide) spanning the many nitrogen oxidation states (from -III up to +V). With referring to the reversible hydrogen electrode potential (RHE), the reduction products would be produced following the reactions below:

$$2\,NO_3^- + 12\,H^+ + 10\,e^- \longrightarrow N_2 + 6\,H_2O \qquad E^0 = 1.25\,V \qquad (1)$$

$$2\,NO_3^- + 10\,H^+ + 8\,e^- \longrightarrow N_2O + 5\,H_2O \qquad E^0 = 1.12\,V \qquad (2)$$

$$NO_3^- + 4\,H^+ + 3\,e^- \longrightarrow NO + 2\,H_2O \qquad E^0 = 0.96\,V \qquad (3)$$

$$NO_3^- + 2\,H^+ + 2\,e^- \longrightarrow NO_2^- + H_2O \qquad E^0 = 0.94\,V \qquad (4)$$

$$NO_3^- + 9\,H^+ + 8\,e^- \longrightarrow NH_3 + 3\,H_2O \qquad E^0 = 0.88\,V \qquad (5)$$

$$NO_3^- + 7\,H^+ + 6\,e^- \longrightarrow NH_2OH + 2\,H_2O \qquad E^0 = 0.73\,V \qquad (6)$$

As for the NO_2^- reduction process:

$$2\,NO_2^- + 8\,H^+ + 6\,e^- \longrightarrow N_2 + 4\,H_2O \qquad E^0 = 1.45\,V \qquad (7)$$

$$2\,NO_2^- + 6\,H^+ + 4\,e^- \longrightarrow N_2O + 3\,H_2O \qquad E^0 = 1.29\,V \qquad (8)$$

$$NO_2^- + 2\,H^+ + e^- \longrightarrow NO + H_2O \qquad E^0 = 1.00\,V \qquad (9)$$

$$NO_2^- + 7\,H^+ + 6\,e^- \longrightarrow NH_3 + 2\,H_2O \qquad E^0 = 0.86\,V \qquad (10)$$

$$NO_2^- + 5\,H^+ + 4\,e^- \longrightarrow NH_2OH + H_2O \qquad E^0 = 0.62\,V \qquad (11)$$

Electrochemical NO reduction reaction has been studied under a variety of reaction conditions, including reactions on different metal electrodes,[23–26] and varying NO concentrations.[23,27] Overall, there are four different products depending on potential observed during

NORR process:

$$2\,NO + 4\,(H^+ + e^-) \longrightarrow N_2 + 2\,H_2O \qquad E^0 = 1.68\,V \tag{12}$$

$$2\,NO + 2\,(H^+ + e^-) \longrightarrow N_2O + H_2O \qquad E^0 = 1.59\,V \tag{13}$$

$$NO + 5\,(H^+ + e^-) \longrightarrow NH_3 + H_2O \qquad E^0 = 0.71\,V \tag{14}$$

$$NO + 3\,(H^+ + e^-) \longrightarrow NH_2OH \qquad E^0 = 0.38\,V \tag{15}$$

Except the reactions mentioned above, the competitive hydrogen evolution reaction (HER) becomes pronounced when potential goes below 0 V vs RHE:

$$2\,(H^+ + e^-) \longrightarrow H_2 \qquad E^0 = 0\,V \tag{16}$$

Thus, below 0 V (vs RHE), the observed Faradaic efficiencies, or percent of electrons used in NORR, can be greatly impacted. All the reactions described above from $NO_3^-/NO_2^-/NO$, illustrate that adsorbed nitric oxide ($*NO$) as divergent center, may control the electrocatalytic selectivity towards N_2O, N_2, NH_2OH and NH_3 as illustrated in Fig. 2. As a result, the affinity to NO on metals will play an essential role in their reduction selectivity performance.

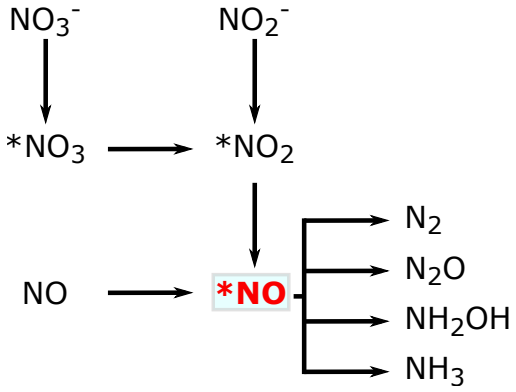

Figure 2: Schematic representation of $NO_3^-/NO_2^-/NO$ reduction pathways.

Results and Discussion

Fig. 1(a) shows for Pt that there are two major reaction regions for NO reduction:

- at low potential ($<$ 0.3 V vs RHE) where both H_2 and NH_3 are observed, and at the potential below 0 V vs RHE, H_2 becomes the main product.
- at high potential (0.3 - 0.7 V vs RHE) which leads to N_2O formation.

Similar potential regions have been observed on other metals, such as Pd, Rh, Ru, Ir and Au. As a comparison, Fig. 1(b) shows Cu producing NH_3 as the main product at low potential ($<$ 0 V vs RHE) and N_2O above 0 V vs RHE.

NORR under Low Potential

To conduct electrocatalytic NO_x reduction on catalysts, NO_x species are expected to be adsorbed on the surfaces. In addition, the competition from HER also has to be avoided, especially under low potential region.

Fig. 3(a) shows the adsorption energies of $*NO_3$ plotted against $*H$ adsorption energy. The horizontal line in Fig. 3(a) shows the equilibrium between NO_3^- and adsorbed $*NO_3$ while the vertical line depicts the equilibrium between $(1/2)H_2$ and adsorbed $*H$ under standard conditions. It is found that almost all metals investigated here can absorb $*NO_3$, except Au (Fig. 3(a)). As a result, all metals, except Au might obtain the electrocatalytic activity for NO_3^- reduction, while on Au, the electroreduction of NO_3^- is hardly detectable as reported experimentally.[16] As for the adsorption of $*H$, there are three binding energy regimes: i) binding $*H$ weakly, limiting availability towards adsorbed $*H$ paves high barrier for their catalytic activity of NO_3^- reduction (Ag/Au); ii) binding $*H$ moderately but still above 0 eV (Cu) and iii) the remaining metals to the left of vertical line bind $*H$ strongly, mainly resulting in HER instead of NO_3^- reduction, especially at potential below 0 V vs RHE.

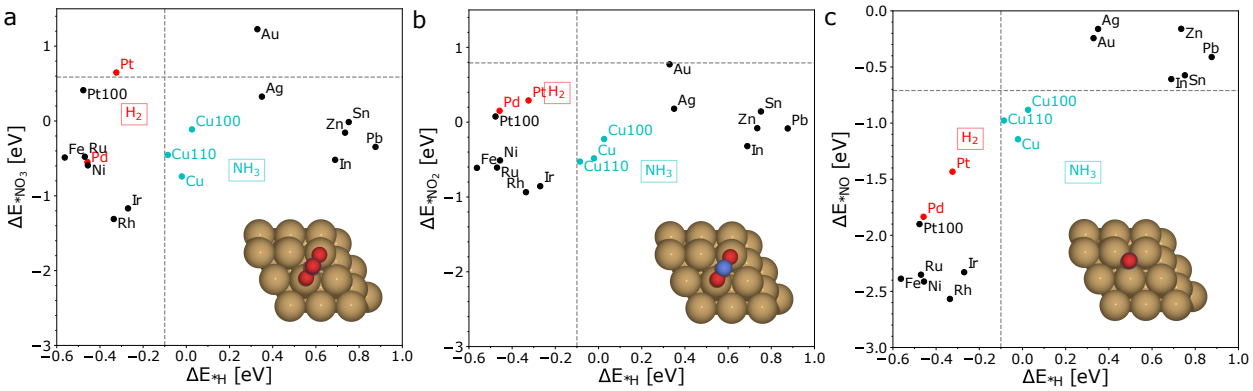

Figure 3: The adsorption energies of the intermediates (a): $\Delta E_{*\mathrm{NO_3}}$; (b) $\Delta E_{*\mathrm{NO_2}}$ and (c) $\Delta E_{*\mathrm{NO}}$ are plotted against $\Delta E_{*\mathrm{H}}$. The horizontal line shows the equilibrium between (a) NO_3^- and adsorbed $*NO_3$; (b) NO_2^- and adsorbed $*NO_2$; (c) NO(gas) and adsorbed $*NO$ while the vertical line depicts the equilibrium between $(1/2)H_2$ and adsorbed $*H$ under standard conditions. Red makers demonstrates H_2 produced as the main product while Cyan color markers shows NH_3 is the main product according to experimental results.[9,10,26,28–30] Here, metals without notification are face-centered cubic (111) structures, except Ru is hcp(0001). Note the effect of the local electric field on the covalent adsorption, including $*NO$ and $*H$ is modest. However, $*NO_3$ and $*NO_2$ is partly influenced by the electric field as shown in Fig. S2.

Fig. 3(b) illustrates the adsorption energies of $*NO_2$ is plotted against $*H$ adsorption energy. The horizontal line shows the equilibrium between NO_2^- and adsorbed $*NO_2$ and again the vertical line describes the equilibrium between $(1/2)H_2$ and adsorbed $*H$. The adsorption tendency towards $*NO_2$ are observed similar to $*NO_3$, except Au. Au binds $*NO_2$ stronger than $*NO_3$, and is close to the equilibrium between NO_2^- and $*NO_2$, leading to some catalytic activity of NO_2^- reduction[18]. Similar to NO_3^- reduction, for NO_2^- reduction, the metals to the left of vertical line binding $*H$ strongly, produces H_2 as the main product under low potential. For the metals to the right of the vertical line, binding $*H$ weakly, like Ag and Au, catalytic NO_2^- reduction is unfavorable due to limiting accessibility of adsorbed $*H$. As for Cu, it adsorbs $*NO_2$ and produces NH_3 with limited HER.

Similar to CO reduction, NORR has been suggested as proton-electron coupled reaction based on the Tafel slope and the pH dependence.[23,25?] As CO reduction has $*CO$ adsorption as a prerequisite descriptor before proton-electron reaction, the NO reduction will have $*NO$ adsorption as a prerequisite descriptor. While, we note that CO_2 reduction directly can

carry out the electron reaction to CO_2^-.[35?] Fig. 3(c) shows the adsorption energies of $*$NO plotted against $*$H adsorption energy. The horizontal line illustrates the equilibrium between NO (gas) and adsorbed $*$NO and the vertical line shows the equilibrium between $(1/2)H_2$ and adsorbed $*$H. Fig. 3(c) illustrates that metals can be classified into three groups in terms of the adsorption energies for $*$NO and $*$H. Metals on the left of vertical line like Pt, Pd, bind both $*$NO and $*$H very strongly, resulting in HER at potential below 0 V vs RHE. On the metals below the horizontal line, the $*$NO binds to the metal surfaces. For the metals on the left of the vertical line, $*$H comes to the surfaces at positive potential. Both these observations lead to partial NH_3 formation at potential just prior to H_2 (H_2 is very slow) and dominant H_2 production with more negative potential applied to these catalysts. This can be seen in some literature.[25,26,31] Taking Ni as an example, few observations of NH_3 has been seen at very low overpotential, before HER.[31] This is in the region where Ni can have $*$H underpotential deposited ($*H_{upd}$) but is not working as sufficient HER catalyst. It is general observation that NH_3 can be formed as the main product at low overpotential when $*$H is present just prior to efficient HER for the catalyst.

For the metals above the horizontal line like Ag and Au, it is unfavourable to bind $*$NO, which limits NO reduction. Indeed, on Ag and Au, NH_3 formation has been reported in limited current.[14,31] This is at potentials where Ag and Au have very low coverage of $*$H, just prior or at the potential for H_2 evolution. At more negative potentials, H_2 becomes the main product when more negative potential is applied.[14] Similar phenomena is reported on Ag and Au for CO_2 reduction where limited methane/methanol is observed.[32,33] These observation indicates that there exists local interesting potential range for NH_3 or CH_4 formation at limited rates on Ag/Au for NORR or CO_2 reduction respectively. However, experiments for NORR also have shown that no NO adsorbate layer on Au is formed and also little formation of NH_3 is observed.[25] In addition, no drastic changes in voltammograms for Ag in Ar and NO was also observed, supporting the limited NORR activity on Ag.[31] Here, only Cu metal binds $*$NO while not having $*H_{upd}$ leading to NH_3 conversion.

The analysis above, shows that NO_x (NO_3^-, NO_2^- and NO) reduction on the metals to the left of the vertical line in Fig. 3 is greatly inhibited by HER, leading to low NO_x product faradic efficiency. For the metals above the horizontal line in Fig. 3(c), NO_x (NO_3^- and NO_2^-) reduction can happen with sufficient potential applied, producing NO while further reduction of NO is hard. Cu stands out with the unique property that it can bind $*NO_3$, $*NO_2$ and *NO but not *H, demonstrating its high selectivity for NO_x reduction over HER. This is similar to CO_2/CO electroreduction (CORR).[21]

Here, the $*NO_x$ vs *H is considered as a selectivity mapping. HER is a competing reaction to NO_x reduction, which is like HER competition with CO_2/CO reduction. What is important is the relative availability of *H and reactant ($*NO_x$ for NO_xRR or *CO for CORR) for the products formation. Experimentally, it is shown that Rh produce H_2 at potential below 0 V for NO_3^- reduction even though $*NO_3$ adsorption is stronger (-1.2 eV) than *H adsorption (-0.35 eV).[34] In addition, similar for CO_2/CO reduction, HER happens on Pt and over 95% FE of H_2 is reported, even though Pt adsorbs *CO (-1.4 eV) much stronger than *H (-0.2 eV).[35] Although NO_x or CO binds stronger at the catalyst in both cases, the availability of *H and hence kinetics for HER is so fast that NO_xRR and CORR is not observed. This correspond to major differences in reaction prefactor for the competing HER and NO_xRR/CORR, resulting in H_2 as primary product. However, the product distribution might change in the different setup, such as gas diffusion electrode (GDE) where NO can have higher chemical potential (pressure).[31] In rotating disk electrode (RDE)/aqueous setup, there is a limitation of the NO solubility (0.0056g/100ml at 20 °C). Due to different setup, GDE and RDE change the availability of *H relative to the reactant *NO on surfaces which again is similar to the situation in CORR where different products distribution is reported in RDE and GDE setups.[36,37]

Fig. 4 demonstrates computational limiting potential for NO reduction towards NH_3 plotted against the adsorption energy of *N (ΔG_{*N}) with the utilization of the scaling relations presented in Fig. S3. The red line represents the strong binding side of the volcano

where the hydrogenation of ∗NH to ∗NHH is limiting step. The blue line shows metals with weak binding of ∗N. For the metals on the weak binding side, ∗NHO is preferred in the protonation of ∗NO, and NH_3 will be produced via ∗NHHO intermediate, leaving ∗O on the surface as shown in Fig. S5. On the weak binding side, Cu prefers ∗NOH while ∗NHO is formed on Ag or Au in the hydrogenation of ∗NO. Further hydrogenation of ∗NOH on Cu produces ∗N and then continuous protonation of ∗N leads to the formation of NH_3. Among all the metals investigated here, Cu is predicted to be the most active catalyst to produce NH_3.

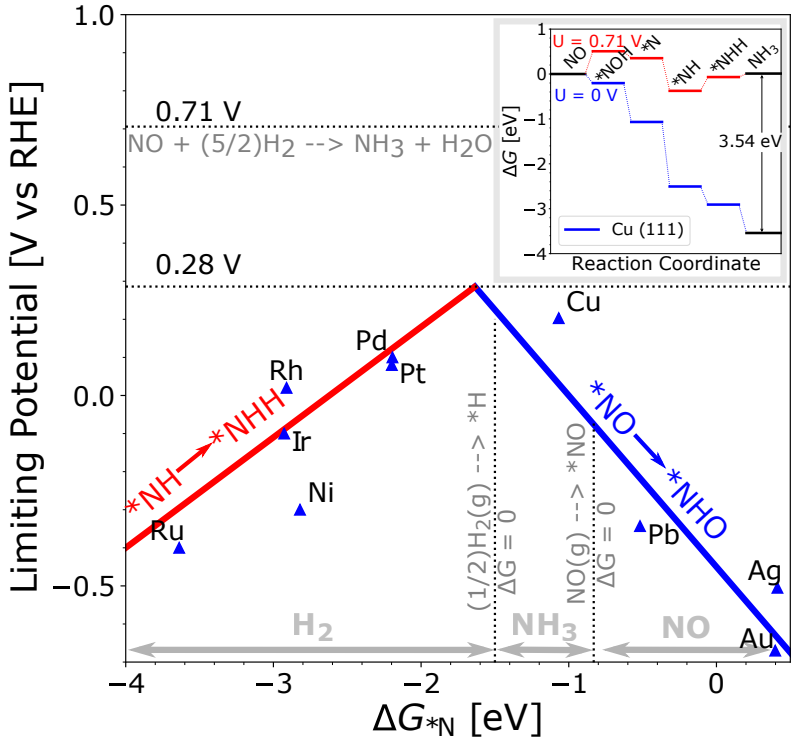

Figure 4: The limiting potential volcano for NO reduction to NH_3. Limiting potential defined as the negative of the free energy change of each proton-coupled electron transfer step, which behaves as a function of the adsorption energy of ∗N (ΔG_{*N}) at 0 V vs RHE. The left red line demonstrates the potential is limited by the strong binding of ∗NH (∗NH towards ∗NHH) while the right blue line shows that the potential is limited by the weak binding of ∗NHO (formation of ∗NHO from ∗NO). The upper dashed horizontal line exhibits the equilibrium potential (0.71 V) which can be obtained from NO reduction to NH_3. The vertical lines shows the ∗H and ∗NO adsorption respectively. Insert: Free energy diagram of NO reduction towards NH_3 on Cu(111), with blue line constructed under 0 V while red line constructed under equilibrium potential (0.71 V). Note Cu is the only metal on the weak binding side but prefers ∗NOH.

A closer catalytic reaction process on Cu(111) can be seen in the insert of Fig. 4. It proceeds via the protonation of the adsorbed $*$NO to $*$NOH intermediate, and further protonation of $*$N and $*$NH leads to NH_3 formation. The first hydrogenation of $*$NO is the potential limiting step. As a result, Cu(111) provides the highest catalytic activity for NH_3 formation among all metals investigated here, and its catalytic activity can be still enhanced by strengthening its $*$N adsorption, since it is still not on the top of the volcano.

Following the scaling relation between $*$N and $*$H and the scaling relation between $*$N and $*$NO shown Fig. S6, the product selectivity (vertical dashed lines) can be also indicated in Fig. 4. When ΔG_{*N} is smaller than -1.5 eV, ΔG_{*H} becomes negative and H_2 will be the main product. For metals with ΔG_{*N} larger than -0.83 eV, the adsorption of $*$NO is unfavorable, leading to the formation of NO. Cu has ΔG_{*N} between -1.5 eV and -0.83 eV, leading to high selectivity for NH_3 production in the process of NORR, as also seen in Fig. Fig. 3.

This computational analysis explains that the experimental results with high faradaic efficiency ($> 90\%$) for NO_x (NO_3^-, NO_2^- and NO) reduction to NH_3 have been achieved on Cu-based catalysts.[10,11,26,38–42] More interestingly, enhanced catalytic activity has also been observed when Cu is alloyed with strong $*$N adsorption metals, like Ni and Rh.[11,39–41] This might be due to the stabilization of $*$NOH intermediate, getting close to the top of the volcano shown in Fig. 4(a) but still ΔG_{*N} in the region of -1.5 eV to -0.83 eV. Fig. 4 shows that there is a very little window to find both selective and active catalyst for the NO reduction in the volcano. Specifically, it hints that we cannot find a metal catalyst that is better than Cu, since it will then become selective toward HER or it will not adsorb NO. At medium potentials (around 0 - 0.3 V vs RHE), the HER is thermodynamically impossible and NH_3 is reported as the major product[25]. With limited access to adsorbed $*$H, much less current density is observed experimentally for the metals.[16,18,25] Still, much higher current density at medium potential is reported on Cu for NO_x (NO_3^-, NO_2^- and NO) reduction under the same experimental conditions, compared to other transition metals.

NORR towards N_2O under High Potential

At high potential region, N_2O formation is observed. For this reaction to occur, N-N coupling is required. Fig. 5(a) shows that the $*$ONNO formation on metals from two NO is unfavourable. More specifically, for strong *NO adsorption metals, two *NO prefer to absorb separately. For metals binding *NO weak like Ag and Au, formation of *ONNO is possible from adsorbed *NO, but adsorption of NO is unfavourable. Experimentally, it has been suggested that solution NO is involved in the reaction sequence to produce N_2O since N_2O is not produced during the reduction of adsorbed $*$NO.[25] It seems more reasonable to speculate N-N bond formation from $*$N and NO. As for the formation of $*$N, besides the continuous protonation of NO_x, the dissociation of NO_x can be another option. Fig. S3 (a-c) present the activation barriers for NO_x dissociation. Ni and Rh have the lowest barriers whereas Ag or Au have the highest barrier. Generally, the barriers for Cu and the platinum group metals is between the two extremes. For the $*NO_x$ (x = 1, 2, and 3) dissociation reactions, E_a increases with decreasing x on a specific metal, implying that the final dissociation step has the highest activation energy. As a result, $*$N might be produced via the dissociation of $*NO_3$ and $*NO_2$ and then the hydrogenation of $*$NO. As for the formation of $*$NO from $*NO_3$ and $*NO_2$ except the direct dissociation mentioned above, the proton-assisted N-O bond cleavage has also been considered. Here, the first protonation of $*NO_3$ and $*NO_2$ shows that molecular HNO_3 or HNO_2 desorb from the surfaces, and potentially these species in solution come back into the NO_3^-/NO_2^- ionic state. A second protonation of HNO_3 or HNO_2 to H_2O and $*NO_2$ or H_2O and $*$NO is possible, but not investigated here.

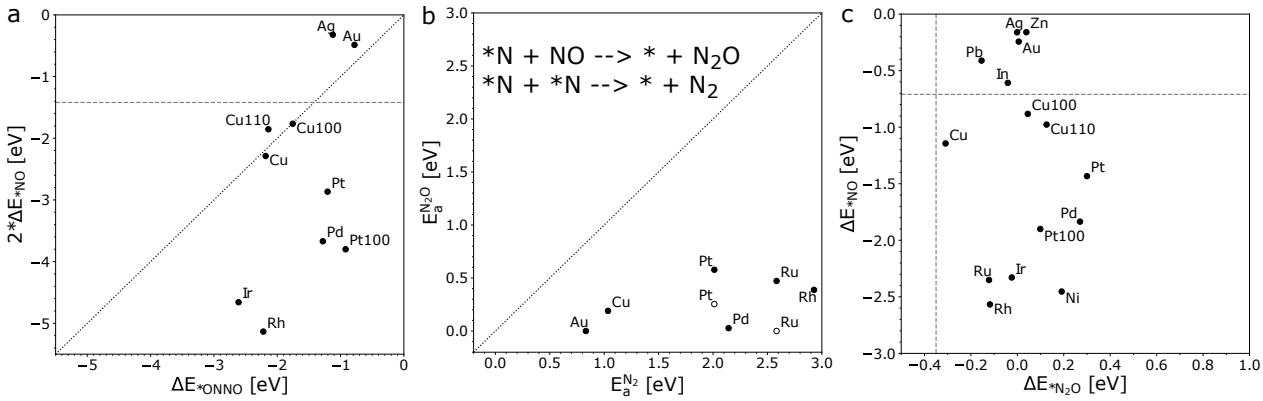

Figure 5: (a)Adsorption energy comparison between twice of ∗NO and N-N coupling intermediate ∗ONNO. The horizontal line shows the equilibrium between 2NO(g) and 2∗NO, while the diagonal line illustrates the equal adsorption energy between 2∗NO and ∗ONNO. (b)The activation barriers for N-N coupling between ∗N and NO (gas) vs ∗N and ∗N. where the unfilled markers show around 0.44 Monolayer of NO coverage is considered. (c) Adsorption energy comparison between ∗NO and ∗N_2O.The horizontal line shows the equilibrium between NO(g) and ∗NO while the vertical line depicts the equilibrium between N_2O and ∗N_2O under standard conditions.

Fig. 5(b) shows the activation barrier for N-N bond formation between adsorbed ∗N and NO plotted against the activation barrier of N_2 formation from two adsorbed ∗N. There is almost no activation observed for N-N coupling between ∗N and NO except Ru, no matter how strong ∗N is adsorbed. Following the experiments, where 0.5 monolayer ∗NO coverage has been suggested on strong adsorption metals like Ru,[25] ∗N and NO coupling becomes feasible with this coverage consideration. In addition, the activation barrier of N_2 formation from adsorbed ∗N is larger than N_2O formation.

Fig. 5(c) shows the adsorption energy comparison between ∗NO and ∗N_2O. The horizontal line shows the equilibrium between NO (gas) and ∗NO while the vertical line depicts the equilibrium between N_2O (gas) and ∗N_2O under standard conditions. It shows that the adsorption of N_2O is not stable for all metals. As a consequence, N_2O will be the main product during NO_x reduction at high potential.

Conclusions

In this study, we use DFT simulations to investigate electrocatalytic NO_x reduction selectivity and activity over metal catalysts. Analogous to classifying CO_2 reduction by $*$CO vs $*$H, we classify metals by the adsorption energy of $*$NO vs $*$H. Since the selectivity of the NO_x reduction is potential dependent, the products formation has been analysed in two different potential regions. At low potential, we think of a general observation, that NH_3 can be formed as the main product when underpotential $*$H is just present on the electrodes. However, trying to increase the reaction rate by slightly more negative potential speeds up HER and gives a significant drop in NH_3 formation, NO_x reduction competes with HER, leading to H_2 as the major product on strong $*$H binding metals. For metals binding $*$H weakly like Ag or Au, NO_3^- and NO_2^- reduction will stop at NO similar to CO_2-to-CO. Cu stands out with the unique property that it can bind $*NO_3$, $*NO_2$ and $*$NO but not having $*H_{upd}$, leading to high selectivity for NH_3 formation.

With the utilization of scaling relations for intermediates adsorption energies, DFT simulated limiting potential is plotted against the adsorption energy of $*$N. Cu is predicted to be the most active metal to conduct NO reduction towards NH_3 and the potential limiting step is the hydrogenation of adsorbed $*$NO. The volcano shows that enhanced activity can be achieved by slightly strengthening the adsorption energy of $*$N on Cu, like alloying Cu with metals binding $*$N stronger but ΔG_{*N} still should be larger than -1.5 eV. At potential between 0 to 0.3 V vs RHE, the limiting adsorbed $*$H results in much less current density compared to that under low potential for NO_x reduction. Still NH_3 is reported as the main product and Cu demonstrates higher current density under the same conditions as compared to other transition metals.

At high potential condition ($>$ 0.3 V vs RHE), high coverage of adsorbed $*$NO is observed for NO reduction. With free NO in the solution, the N-N bond formation from adsorbed $*$N and NO, forming N_2O, is feasible while it is impossible to produce N_2 via the association of two adsorbed $*$N.

These descriptor-based analyses in this work provide a description of the NO reduction or even NO_3^- and NO_2^- reduction network on metals at atomic scale. These findings offer a guidance or inspiration for the design and discovery of both selective and active NO_x (NO_3^-, NO_2^- and NO) reduction electrocatalysts.

Computational Details

The computational analysis was carried out using the grid-based projector-augmented wave (GPAW) method, a DFT code based on a projected augmented wave (all-electron frozen core approximation) method integrated with the atomic simulation environment (ASE).[43–45] The revised Perdew-Burke-Ernzerhof (RPBE) functional was used as an exchange-correlation functional.[46] The wavefunctions were represented on a uniform real-spaced grid with 0.18 Å grid-spacing. Monkhorst-Pack k-points sampling of $3 \times 3 \times 1$ were used for all calculations. The electronic spins are treated separately, and a vacuum of minimum 7 Å was employed. Besides the calculation for climbing image nudged elastic band (NEB) was performed with GPAW code.[47] The quasi-Newton minimization scheme was employed for the geometry optimizations, and the systems were relaxed until the forces were less than 0.05 eV/ Å. The metal structures (except Ru which is hexagonal close-packed (0001)) are composed of 111 surface slab face-centered cubic (FCC) $3 \times 3 \times 4$ unit cell, with fixed two bottom layers. For Pt and Cu, other facets, FCC Pt(110), Cu(110) and Cu(100) are also considered in the classification. The $*NO_3$ and $*NO_2$ adsorption energies are calculated with respect to nitrate ions (NO_3^-) and nitrite ions (NO_2^-) respectively in solution, as shown in Fig. S1. The way of computing the free energies from DFT values, including details of zero-point energies, entropies and other additional corrections, is shown in the Supporting Information. Structures, total energies, scripts to run calculations, and plotting methods are collected in the KatlaDB database available at this link: `https://nano.ku.dk/english/research/theoretical-electrocatalysis/katladb/`.

Acknowledgement

We acknowledge support from the Danish Council for Independent Research Sapere Aude Program, Grant No. 11-1051390, research grant 9455 from VILLUM FONDEN and Innovation Fund Denmark (grand solution ProActivE 5124-00003A). The Center for High Entropy Alloys Catalysis is sponsored by the Danish National Research Foundation centers of excellence, Project DNRF149.

References

(1) Galloway, J. N.; Townsend, A. R.; Erisman, J. W.; Bekunda, M.; Cai, Z.; Freney, J. R.; Martinelli, L. A.; Seitzinger, S. P.; Sutton, M. A. Transformation of the Nitrogen Cycle: Recent Trends, Questions, and Potential Solutions. *Science* **2008**, *320*, 889–892.

(2) Canfield, D. E.; Glazer, A. N.; Falkowski, P. G. The Evolution and Future of Earth's Nitrogen Cycle. *Science* **2010**, *330*, 192–196.

(3) Cole, J. A.; Benjamin, N.; Lundberg, J. O.; Weitzberg, E. Nitrate, bacteria and human health. *Nature reviews. Microbiology* **2004**, *2*, 593–602.

(4) Gruber, N.; Galloway, J. N. An Earth-system perspective of the global nitrogen cycle. *Nature* **2008**, *451*, 293–296.

(5) Pennino, M. J.; Compton, J. E.; Leibowitz, S. G. Trends in Drinking Water Nitrate Violations Across the United States. *Environ. Sci. Technol.* **2017**, *51*, 13450–13460.

(6) Rosca, V.; Duca, M.; de Groot, M. T.; Koper, M. T. M. Nitrogen Cycle Electrocatalysis. *Chem. Rev.* **2009**, *109*, 2209–2244, DOI: 10.1021/cr8003696.

(7) Duca, M.; Koper, M. T. M. Powering denitrification: the perspectives of electrocatalytic nitrate reduction. *Energy Environ. Sci.* **2012**, *5*, 9726–9742, DOI: 10.1039/C2EE23062C.

(8) Bae, S.-E.; Stewart, K. L.; Gewirth, A. A. Nitrate Adsorption and Reduction on Cu(100) in Acidic Solution. *J. Am. Chem. Soc.* **2007**, *129*, 10171–10180, DOI: 10.1021/ja071330n, PMID: 17655297.

(9) Garcia-Segura, S.; Lanzarini-Lopes, M.; Hristovski, K.; Westerhoff, P. Electrocatalytic reduction of nitrate: Fundamentals to full-scale water treatment applications. *Appl. Catal. B* **2018**, *236*, 546–568, DOI: 10.1016/j.apcatb.2018.05.041.

(10) Wang, Y.; Zhou, W.; Jia, R.; Yu, Y.; Zhang, B. Unveiling the Activity Origin of a Copper-based Electrocatalyst for Selective Nitrate Reduction to Ammonia. *Angew. Chem. Int. Ed.* **2020**, *59*, 5350–5354.

(11) Wang, Y.; Xu, A.; Wang, Z.; Huang, L.; Li, J.; Li, F.; Wicks, J.; Luo, M.; Nam, D.-H.; Tan, C.-S.; Ding, Y.; Wu, J.; Lum, Y.; Dinh, C.-T.; Sinton, D.; Zheng, G.; Sargent, E. H. Enhanced Nitrate-to-Ammonia Activity on Copper-Nickel Alloys via Tuning of Intermediate Adsorption. *J. Am. Chem. Soc.* **2020**, *142*, 5702–5708, DOI: 10.1021/jacs.9b13347, PMID: 32118414.

(12) van Langevelde, P. H.; Katsounaros, I.; Koper, M. T. Electrocatalytic Nitrate Reduction for Sustainable Ammonia Production. *Joule* **2021**, *5*, 290–294, DOI: https://doi.org/10.1016/j.joule.2020.12.025.

(13) Li, P.; Jin, Z.; Fang, Z.; Yu, G. A single-site iron catalyst with preoccupied active centers that achieves selective ammonia electrosynthesis from nitrate. *Energy Environ. Sci.* **2021**, –, DOI: 10.1039/D1EE00545F.

(14) Kim, D.; Shin, D.; Heo, J.; Lim, H.; Lim, J.-A.; Jeong, H. M.; Kim, B.-S.; Heo, I.; Oh, I.; Lee, B.; Sharma, M.; Lim, H.; Kim, H.; Kwon, Y. Unveiling Electrode–Electrolyte Design-Based NO Reduction for NH3 Synthesis. *ACS Energy Lett.* **2020**, *5*, 3647–3656, DOI: 10.1021/acsenergylett.0c02082.

(15) Wu, Z.-Y.; Karamad, M.; Yong, X.; Huang, Q.; Cullen, D. A.; Zhu, P.; Xia, C.; Xiao, Q.; Shakouri, M.; Chen, F.-Y.; Kim, J. Y.; Xia, Y.; Heck, K.; Hu, Y.; Wong, M. S.; Li, Q.; Gates, I.; Siahrostami, S.; Wang, H. Electrochemical ammonia synthesis via nitrate reduction on Fe single atom catalyst. *Nat. commun.* **2021**, *12*.

(16) Dima, G.; de Vooys, A.; Koper, M. Electrocatalytic reduction of nitrate at low concentration on coinage and transition-metal electrodes in acid solutions. *J. electroanal. chem.* **2003**, *554-555*, 15–23.

(17) de Groot, M.; Koper, M. The influence of nitrate concentration and acidity on the electrocatalytic reduction of nitrate on platinum. *J. electroanal. chem.* **2004**, *562*, 81–94.

(18) Duca, M.; van der Klugt, B.; Koper, M. Electrocatalytic reduction of nitrite on transition and coinage metals. *Electrochimica Acta* **2012**, *68*, 32–43, DOI: 10.1016/j.electacta.2012.02.037.

(19) Chun, H.-J.; Apaja, V.; Clayborne, A.; Honkala, K.; Greeley, J. Atomistic Insights into Nitrogen-Cycle Electrochemistry: A Combined DFT and Kinetic Monte Carlo Analysis of NO Electrochemical Reduction on Pt(100). *ACS Catal.* **2017**, *7*, 3869–3882, DOI: 10.1021/acscatal.7b00547.

(20) Casey-Stevens, C. A.; Ásmundsson, H.; Skúlason, E.; Garden, A. L. A density functional theory study of the mechanism and onset potentials for the major products of NO electroreduction on transition metal catalysts. *Applied Surface Science* **2021**, *552*, 149063, DOI: 10.1016/j.apsusc.2021.149063.

(21) Bagger, A.; Ju, W.; Varela, A. S.; Strasser, P.; Rossmeisl, J. Electrochemical CO2 Reduction: A Classification Problem. *ChemPhysChem* **2017**, *18*, 3266–3273, DOI: 10.1002/cphc.201700736.

(22) Wan, H.; Jiao, Y.; Bagger, A.; Rossmeisl, J. Three-Dimensional Carbon Electrocatalysts for CO2 or CO Reduction. *ACS Catal.* **2021**, *11*, 533–541, DOI: 10.1021/acscatal.0c04878.

(23) de Vooys, A.; Koper, M.; van Santen, R.; van Veen, J. Mechanistic study of the nitric oxide reduction on a polycrystalline platinum electrode. *Electrochim. acta* **2001**, *46*, 923–930.

(24) de Vooys, A.; Beltramo, G.; van Riet, B.; van Veen, J.; Koper, M. Mechanisms of electrochemical reduction and oxidation of nitric oxide. *Electrochim. acta* **2004**, *49*, 1307–1314.

(25) de Vooys, A.; Koper, M.; van Santen, R.; van Veen, J. Mechanistic Study on the Electrocatalytic Reduction of Nitric Oxide on Transition-Metal Electrodes. *J. catal.* **2001**, *202*, 387–394.

(26) Long, J.; Chen, S.; Zhang, Y.; Guo, C.; Fu, X.; Deng, D.; Xiao, J. Direct Electrochemical Ammonia Synthesis from Nitric Oxide. *Angew. Chem., Int. Ed.* **2020**, *59*, 9711–9718.

(27) Cuesta, A.; Escudero, M. Electrochemical and FTIRS characterisation of NO adlayers on cyanide-modified Pt(111) electrodes: the mechanism of nitric oxide electroreduction on Pt. *Phys. Chem. Chem. Phys.* **2008**, *10*, 3628–.

(28) Pérez-Gallent, E.; Figueiredo, M. C.; Katsounaros, I.; Koper, M. T. Electrocatalytic reduction of Nitrate on Copper single crystals in acidic and alkaline solutions. *Electrochimica Acta* **2017**, *227*, 77–84, DOI: 10.1016/j.electacta.2016.12.147.

(29) Hasnat, M.; Ben Aoun, S.; Nizam Uddin, S.; Alam, M.; Koay, P.; Amertharaj, S.; Rashed, M.; Rahman, M. M.; Mohamed, N. Copper-immobilized platinum electrocatalyst for the effective reduction of nitrate in a low conductive medium: Mechanism,

adsorption thermodynamics and stability. *Applied Catalysis A: General* **2014**, *478*, 259–266, DOI: 10.1016/j.apcata.2014.04.017.

(30) Soto-Hernández, J.; Santiago-Ramirez, C.; Ramirez-Meneses, E.; Luna-Trujillo, M.; Wang, J.-A.; Lartundo-Rojas, L.; Manzo-Robledo, A. Electrochemical reduction of NOx species at the interface of nanostructured Pd and PdCu catalysts in alkaline conditions. *Applied Catalysis B: Environmental* **2019**, *259*, 118048, DOI: 10.1016/j.apcatb.2019.118048.

(31) Hara, K.; Kamata, M.; Sonoyama, N.; Sakata, T. Electrocatalytic reduction of NO on metal electrodes and gas diffusion electrodes in an aqueous electrolyte. *Journal of Electroanal. Chem.* **1998**, *451*, 181–186, DOI: https://doi.org/10.1016/S0022-0728(98)00079-5.

(32) Kuhl, K. P.; Hatsukade, T.; Cave, E. R.; Abram, D. N.; Kibsgaard, J.; Jaramillo, T. F. Electrocatalytic Conversion of Carbon Dioxide to Methane and Methanol on Transition Metal Surfaces. *J. Am. Chem. Soc.* **2014**, *136*, 14107–14113, DOI: 10.1021/ja505791r, PMID: 25259478.

(33) Dutta, A.; Morstein, C. E.; Rahaman, M.; Cedeño López, A.; Broekmann, P. Beyond Copper in CO2 Electrolysis: Effective Hydrocarbon Production on Silver-Nanofoam Catalysts. *ACS Catal.* **2018**, *8*, 8357–8368, DOI: 10.1021/acscatal.8b01738.

(34) Yao, Y.; Zhu, S.; Wang, H.; Li, H.; Shao, M. A Spectroscopic Study of Electrochemical Nitrogen and Nitrate Reduction on Rhodium Surfaces. *Angew. Chem., Int. Ed.* **2020**, *59*, 10479–10483, DOI: 10.1002/anie.202003071.

(35) Hori, Y.; Murata, A.; Takahashi, R. Formation of hydrocarbons in the electrochemical reduction of carbon dioxide at a copper electrode in aqueous solution. *J. Chem. Soc., Faraday Trans. 1* **1989**, *85*, 2309–2326, DOI: 10.1039/F19898502309.

(36) Nakagawa, S.; Kudo, A.; Azuma, M.; Sakata, T. Effect of pressure on the electrochemical reduction of CO2 on Group VIII metal electrodes. *Journal of Electroanal. Chem. and Interfacial Electrochem.* **1991**, *308*, 339–343, DOI: https://doi.org/10.1016/0022-0728(91)85080-9.

(37) Hara, K.; Kudo, A.; Sakata, T. Electrochemical reduction of carbon dioxide under high pressure on various electrodes in an aqueous electrolyte. *Journal of Electroanal. Chem.* **1995**, *391*, 141–147, DOI: 10.1016/0022-0728(95)03935-A.

(38) Reyter, D.; Chamoulaud, G.; Bélanger, D.; Roué, L. Electrocatalytic reduction of nitrate on copper electrodes prepared by high-energy ball milling. *J. Electroanal. Chem.* **2006**, *596*, 13–24, DOI: 10.1016/j.jelechem.2006.06.012.

(39) Comisso, N.; Cattarin, S.; Fiameni, S.; Gerbasi, R.; Mattarozzi, L.; Musiani, M.; Vázquez-Gómez, L.; Verlato, E. Electrodeposition of Cu-Rh alloys and their use as cathodes for nitrate reduction. *Electrochem. Commun.* **2012**, *25*, 91–93, DOI: 10.1016/j.elecom.2012.09.026.

(40) Mattarozzi, L.; Cattarin, S.; Comisso, N.; Guerriero, P.; Musiani, M.; Vázquez-Gómez, L.; Verlato, E. Electrochemical reduction of nitrate and nitrite in alkaline media at CuNi alloy electrodes. *Electrochim. Acta* **2013**, *89*, 488–496, DOI: 10.1016/j.electacta.2012.11.074.

(41) Mattarozzi, L.; Cattarin, S.; Comisso, N.; Gambirasi, A.; Guerriero, P.; Musiani, M.; Vázquez-Gómez, L.; Verlato, E. Hydrogen evolution assisted electrodeposition of porous Cu-Ni alloy electrodes and their use for nitrate reduction in alkali. *Electrochim. Acta* **2014**, *140*, 337–344, DOI: 10.1016/j.electacta.2014.04.048, Electrochemistry for a New Era.

(42) Sun, J.; Alam, D.; Daiyan, R.; Masood, H.; Zhang, T.; Zhou, R.; Cullen, P. J.; Lovell, E. C.; Jalili, A. R.; Amal, R. A hybrid plasma electrocatalytic process for

sustainable ammonia production. *Energy Environ. Sci.* **2021**, *14*, 865–872, DOI: 10.1039/D0EE03769A.

(43) Mortensen, J. J.; Hansen, L. B.; Jacobsen, K. W. Real-space grid implementation of the projector augmented wave method. *Phys. Rev. B* **2005**, *71*, 035109, DOI: 10.1103/PhysRevB.71.035109.

(44) Larsen, A. H.; Mortensen, J. J.; Blomqvist, J.; Castelli, I. E.; Christensen, R.; Dułak, M.; Friis, J.; Groves, M. N.; Hammer, B.; Hargus, C.; Hermes, E. D.; Jennings, P. C.; Jensen, P. B.; Kermode, J.; Kitchin, J. R.; Kolsbjerg, E. L.; Kubal, J.; Kaasbjerg, K.; Lysgaard, S.; Maronsson, J. B.; Maxson, T.; Olsen, T.; Pastewka, L.; Peterson, A.; Rostgaard, C.; Schiøtz, J.; Schütt, O.; Strange, M.; Thygesen, K. S.; Vegge, T.; Vilhelmsen, L.; Walter, M.; Zeng, Z.; Jacobsen, K. W. The atomic simulation environment—a Python library for working with atoms. *J. Phys.: Condens. Matter* **2017**, *29*, 273002.

(45) Bahn, S. R.; Jacobsen, K. W. An object-oriented scripting interface to a legacy electronic structure code. *Comput. Sci. Eng.* **2002**, *4*, 56–66, DOI: 10.1109/5992.998641.

(46) Hammer, B.; Hansen, L. B.; Nørskov, J. K. Improved adsorption energetics within density-functional theory using revised Perdew-Burke-Ernzerhof functionals. *Phys. Rev. B* **1999**, *59*, 7413–7421, DOI: 10.1103/PhysRevB.59.7413.

(47) Henkelman, G.; Uberuaga, B. P.; Jónsson, H. A climbing image nudged elastic band method for finding saddle points and minimum energy paths. *J. Chem. Phys.* **2000**, *113*, 9901–9904, DOI: 10.1063/1.1329672.

Graphical TOC Entry

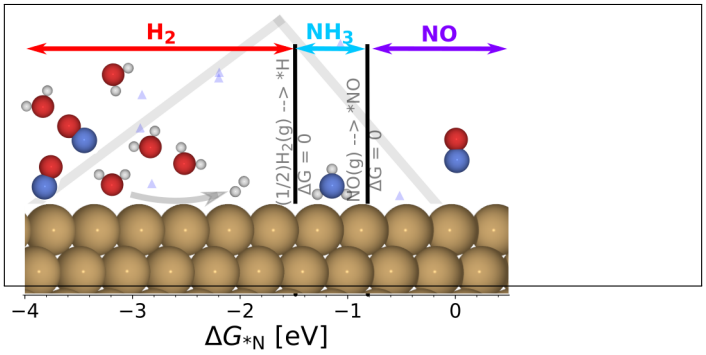

Illustration of selectivity and activity on metals for nitric oxide reduction reaction